Electronic Supplementary Material (ESI) for Inorganic Chemistry Frontiers.
This journal is © the Partner Organisations 2022

Water-driven reversible switching of single-ion magnetism in a dysprosium sulfonate

Dong Shao, [a,e]* Wanjie Tang, [a] Zhijun Ruan, [a] Xiaodong Yang, [a] Le Shi, [d] Xiao-Qin Wei, *[b] Zhengfang Tian, [a] Kusum Kumari [c] and Saurabh Kumar Singh*[c]

[a] Hubei Key Laboratory of Processing and Application of Catalytic Materials, College of Chemistry and Chemical Engineering, Huanggang Normal University, Huanggang 438000, P. R. China

[b] Department of Material Science and Engineering, Shanxi Province Collaborative Innovation Center for Light Materials Modification and Application, Jinzhong University, Jinzhong, 030619, P. R. China.

[c] Department of Chemistry, Indian Institute of Technology Hyderabad, Kandi-502285, Sangareddy, Telangana, India.

[d] State Key Laboratory of Chemical Engineering, Stoddart Institute of Molecular Science, Department of Chemistry, Zhejiang University, Hangzhou 310027, P. R. China.

[e] State Key Laboratory of Coordination Chemistry, Nanjing University, Nanjing, 210023, P. R. China.

Email: shaodong@nju.edu.cn; sksingh@chy.iith.ac.in

Table of Content

Experimental Section

General Procedure. Powder X-ray diffraction data (PXRD) were recorded on a Bruker D8 Advance diffractometer with Cu Kα X-ray source (λ = 1.54056 Å) operated at 40 kV and 40 mA. Simulated PXRD pattern was obtained from the Mercury software. Infrared spectra (IR) data were measured on KBr pellets using a Nexus 870 FT-IR spectrometer in the range of 4000-400 cm^{-1}. Elemental analyses of C, H, and N were performed at an Elementar Vario MICRO analyzer. Thermal gravimetric analysis (TGA) was measured in Al_2O_3 crucibles using a PerkinElmer Thermal Analysis in the temperature range of 30-600 °C under an argon atmosphere. Proton conductivity measurements were performed using a quasi-four-electrode AC impedance technique with a Solartron 1260 impedance/gain-phase analyzer. The single crystals samples were compressed to 2.5 mm diameter, which were connected to gold wires using silver paste. The sample pellet was measured at a frequency range of 1 Hz to 1 GHz in the temperature range of 25−110 °C and in different RH. The conductivity of the samples was deduced from the Debye semicircle in the Nyquist plot.

Magnetic Measurements. Magnetic susceptibility measurements from 2 to 300 K with dc field up to 70 kOe were performed using a Quantum Design SQUID VSM magnetometer on the grounded powders from the single crystals of the compounds. Alternative current (ac) magnetic susceptibility data were collected in zero direct current (dc) field or 1000 Oe dc field in the temperature range of 2-20 K, under an ac field of 2 Oe, oscillating at frequencies in the range of 1-1000 Hz. All magnetic data were corrected for the diamagnetism of the sample holder and of the diamagnetic contribution of the sample using Passcal's constants.

X-ray Crystallography. Single crystal X-ray crystallographic data were collected on a Bruker D8 Venture diffractometer with a CCD area detector (Mo-Kα radiation, λ = 0.71073 Å) at different temperature controlled by Oxford Cryosystems low-temperature device. The unit cell parameters and data collection were determined by the APEXII program. The data were integrated and corrected for Lorentz and polarization effects using SAINT.[S1] Absorption corrections were applied with SADABS.[S2] The structures

were solved by direct methods and refined by full-matrix least-squares method on *F*2 using the SHELXTL[S3] crystallographic software package integrated in Olex 2.[S4] All the non-hydrogen atoms were refined anisotropically. Hydrogen atoms of the organic ligands were refined as riding on the corresponding non-hydrogen atoms. Additional details of the data collections and structural refinement parameters are provided in Table 1. Selected bond lengths and angles of **1**·3H_2O and **1**·H_2O are listed in Table S1 and S2. CCDC 2196277 (150 K), 2196278 (300 K), 2196279 (353 K), and 2196280 (400 K) are the supplementary crystallographic data for this paper. They can be obtained freely from the Cambridge Crystallographic Data Centre via www.ccdc.cam.ac.uk/data_request/cif.

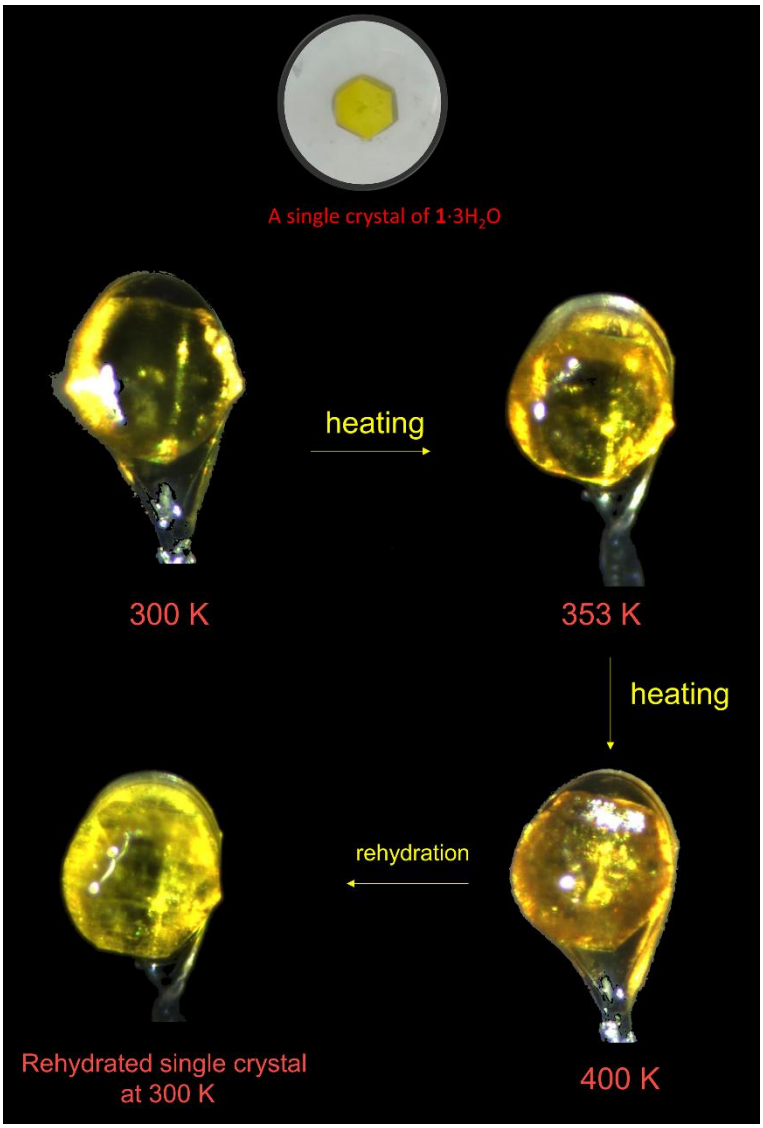

Figure S1. The photographs of a single crystal of **1**·3H_2O, the single crystal in X-ray diffractometer at different temperature, and the rehydrated single crystal at 300 K.

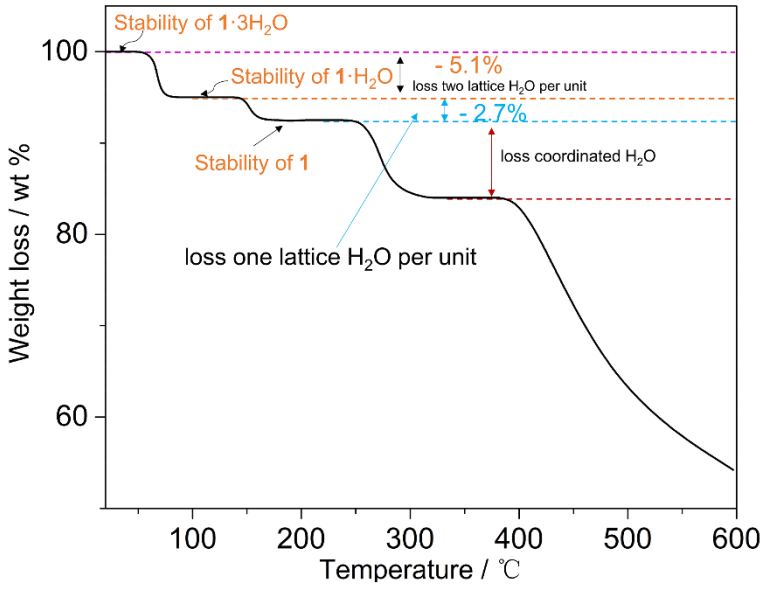

Figure S2. Thermal gravimetric analysis of **1**·3H_2O.

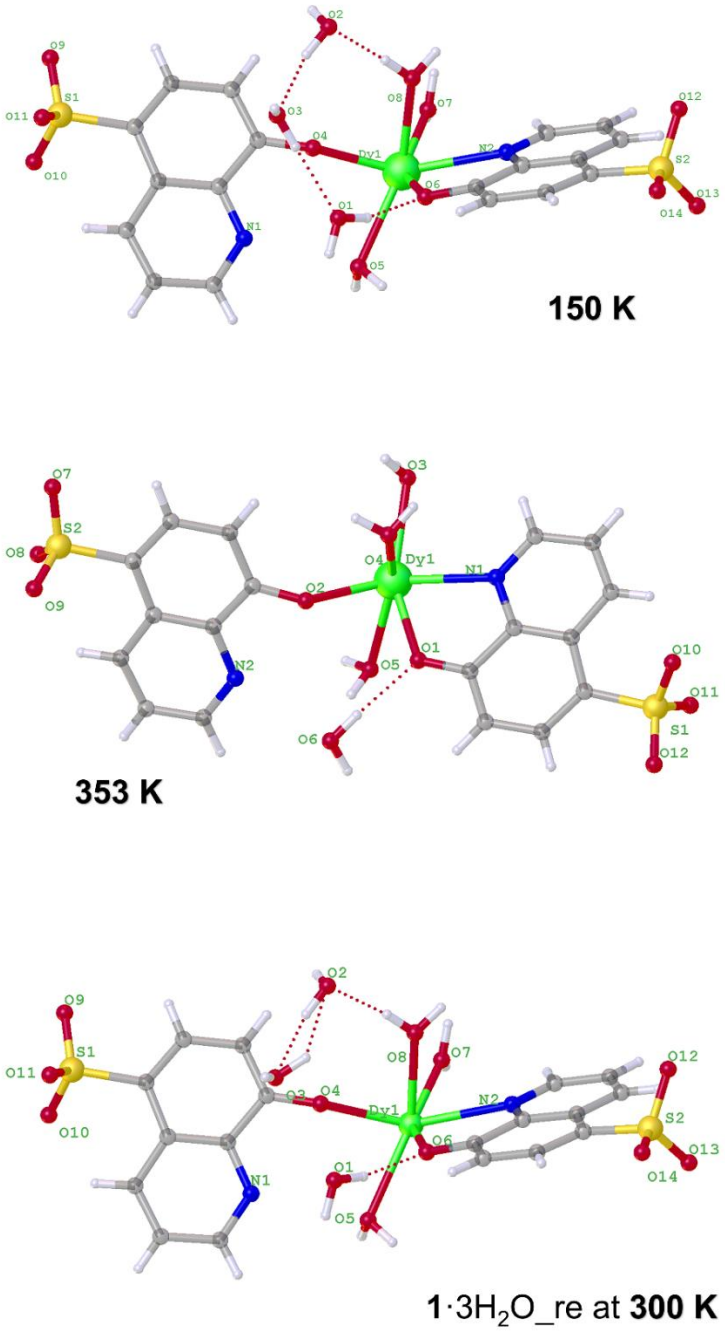

Figure S3. The asymmetric units of **1**·3H_2O at 150 K, **1**·H_2O at 353 K and **1**·3H_2O_re at 300 K.

Table S1. Selected bond lengths (Å) and angles [°] for **1**·3H_2O.

Parameter	Value / Å, °	
T / K	**150**	**300**
Dy1-O4	2.2286(14)	2.2306(15)
Dy1-O5	2.4856(15)	2.4878(16)
Dy1-O6	2.2817(15)	2.2808(15)
Dy1-O7	2.3678(15)	2.3726(17)
Dy1-O8	2.3650(16)	2.3722(18)
Dy1-O10^{1}	2.4100(15)	2.4107(15)
Dy1-O13^{2}	2.3232(15)	2.3247(16)
Dy-$O_{average}$	2.3517	2.3542
Dy1-N2	2.5380(17)	2.5412(17)
O4-Dy1-O5	77.36(5)	77.12(6)
O4-Dy1-O6	90.15(5)	90.07(6)
O4-Dy1-O7	108.81(6)	108.27(7)
O4-Dy1-O8	75.76(5)	75.49(6)
O4-Dy1-O10^{1}	75.15(5)	75.66(6)
O4-Dy1-O13^{2}	145.76(6)	146.08(6)
O5-Dy1-N2	119.63(5)	119.98(5)
O7-Dy1-O5	142.84(5)	142.96(6)
O7-Dy1-O10^{1}	74.15(5)	73.73(6)
O7-Dy1-N2	79.25(6)	79.60(6)
O6-Dy1-N2	66.99(5)	66.87(6)
O8-Dy1-O5	140.10(5)	140.32(6)
O8-Dy1-O7	74.59(6)	73.79(7)

Table S2. Selected bond lengths (Å) and angles [°] for **1**·H_2O.

Parameter	Value / Å, °	
T / K	**353**	**400**
Dy1-O1	2.254(3)	2.238(5)
Dy1-O2	2.230(3)	2.233(5)
Dy1-O3	2.403(4)	2.391(7)
Dy1-O4	2.450(4)	2.441(7)
Dy1-O5	2.528(5)	2.611(10)
Dy1-O8^1	2.349(3)	2.342(6)
Dy1-O11^2	2.295(3)	2.281(6)
Dy-$O_{average}$	2.358	2.352
Dy1-N1	2.539(3)	2.532(6)
O1-Dy1-O3	145.37(13)	146.0(3)
O1-Dy1-O4	84.35(13)	85.8(2)
O1-Dy1-O5	70.54(15)	69.5(3)
O1-Dy1-O8^1	139.75(13)	138.8(2)
O1-Dy1-O11^2	106.78(13)	104.5(2)
O1-Dy1-N1	66.72(11)	67.03(18)
O2-Dy1-O1	82.77(12)	81.9(2)
O2-Dy1-N1	136.99(12)	136.9(2)
O3-Dy1-O4	70.83(14)	70.5(3)
O3-Dy1-N1	82.99(13)	82.7(2)
O5-Dy1-N1	114.09(15)	113.4(3)
O8^1-Dy1-O3	74.83(15)	75.3(3)
O11^2-Dy1-O4	137.08(14)	138.1(2)

Table S3. Continuous Shape Measure (CSM) analysis for eight-coordinated Dy(III) in **1**·3H_2O and **1**·H_2O.

Eight-coordinated coordination sphere label	Symmetry	CSM parameters				Determined coordination geometry
		1·3H_2O		**1**·H_2O		
T / K		**150**	**300**	**353**	**400**	
OP-8	D_{8h}	29.999	30.119	30.959	30.837	
HPY-8	C_{7v}	22.694	22.639	22.225	22.270	
HBPY-8	D_{6h}	15.267	15.132	14.287	14.456	
CU-8	O_h	11.006	11.023	8.683	8.774	
SAPR-8	**D_{4d}**	**1.027**	**1.052**	**0.909**	**0.856**	**SAPR-8**
TDD-8	D_{2d}	1.315	1.305	2.738	2.647	
JGBF-8	D_{2d}	12.769	12.557	13.293	13.443	
JETBPY-8	D_{3h}	26.913	27.125	26.975	27.195	
JBTP-8	C_{2v}	1.679	1.692	2.016	1.909	
BTPR-8	C_{2v}	1.643	1.677	2.259	2.151	
JSD-8	D_{2d}	2.711	2.700	4.101	4.015	
TT-8	T_d	11.588	11.604	9.082	9.186	
ETBPY-8	D_{3h}	23.695	23.881	23.051	23.331	

OP-8 Octagon
HPY-8 Heptagonal pyramid
HBPY-8 Hexagonal bipyramid
CU-8 Cube
SAPR-8 Square antiprism
TDD-8 Triangular dodecahedron
JGBF-8 Johnson - Gyrobifastigium (J26)
JETBPY-8 Johnson - Elongated triangular bipyramid (J14)
JBTP-8 Johnson - Biaugmented trigonal prism (J50)
BTPR-8 Biaugmented trigonal prism
JSD-8 Snub disphenoid (J84)
TT-8 Triakis tetrahedron
ETBPY-8 Elongated trigonal bipyramid (see 8)

Table S4. Crystal Data and Structure Parameters for compound **1**·3H_2O_re.

Complex	**1**·3H_2O_re
formula	$C_{18}H_{22}DyN_2O_{14}S_2$
formula weight	716.99
temperature/K	293
crystal system	monoclinic
space group	*P2₁/n*
a/Å	8.6606(7)
b/Å	14.3467(10)
c/Å	18.6998(12)
α/°	90
β/°	92.713(3)
γ/°	90
Volume/Å^3	2320.9(3)
Z	4
ρcalcg/cm^3	2.052
μ/mm^{-1}	3.478
F(000)	1416.0
R_{int} / R_{sigma}	0.0875 / 0.0294
Goodness-of-fit on F^2	1.132
R_1[a] / wR_2[b] (I > 2σ(I))	0.0372 / 0.0724
R_1/ wR_2 (all data)	0.0532 / 0.0789
Max/min [e Å^{-3}]	1.39 / -1.70

[a]$R_1 = \sum||F_o| - |F_c||/\sum|F_o|$ [b] $wR_2 = \{\sum[w(F_o^2 - F_c^2)2]/\sum[w(F_o^2)^2]\}^{1/2}$

Table S5. Selected bond lengths (Å) and angles [°] for **1**·3H_2O_re.

Parameter	Value / Å, °
T / K	**300**
Dy1-O4	2.233(4)
Dy1-O5	2.490(4)
Dy1-O6	2.279(3)
Dy1-O7	2.366(4)
Dy1-O8	2.372(4)
Dy1-O10^{1}	2.407(4)
Dy1-O13^{2}	2.323(4)
Dy-$O_{average}$	2.353
Dy1-N2	2.544(4)
O4-Dy1-O5	77.28(14)
O4-Dy1-O6	90.00(14)
O4-Dy1-O7	108.24(17)
O4-Dy1-O8	75.24(15)
O4-Dy1-O10^{1}	75.58(14)
O4-Dy1-O13^{2}	146.11(15)
O5-Dy1-N2	119.87(14)
O7-Dy1-O5	142.99(14)
O7-Dy1-O10^{1}	73.61(15)
O7-Dy1-N2	79.65(15)
O6-Dy1-N2	66.79(13)
O8-Dy1-O5	140.59(15)
O8-Dy1-O7	73.42(16)

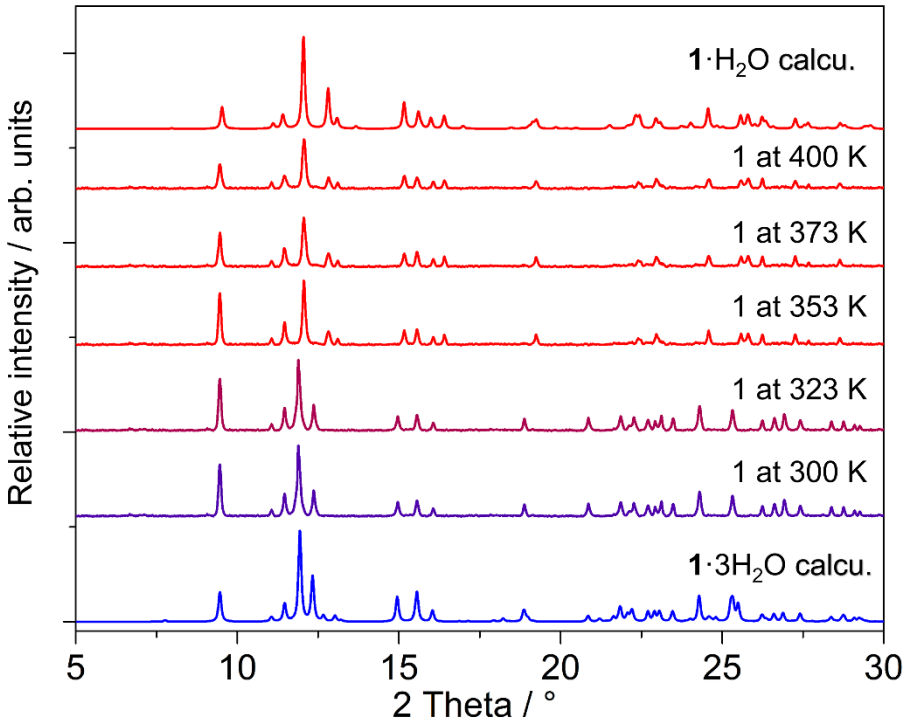

Figure S4. Temperature dependence of the powder X-ray diffraction (PXRD) patterns for **1**·3H_2O. The respective simulated PXRD patterns of **1**·3H_2O and **1**·H_2O were calculated on the basis of the single-crystal data via Mercury.

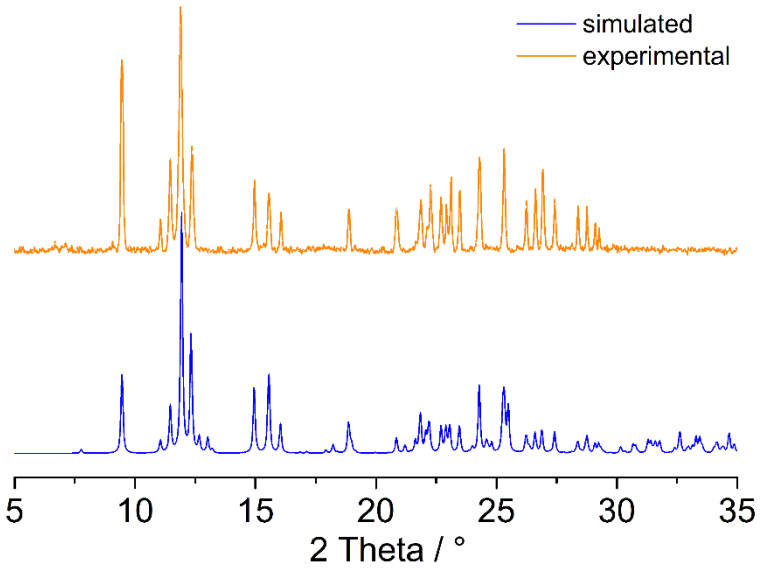

Figure S5. The experimental PXRD for rehydrated crystal sample of **1**·3H_2O_re.

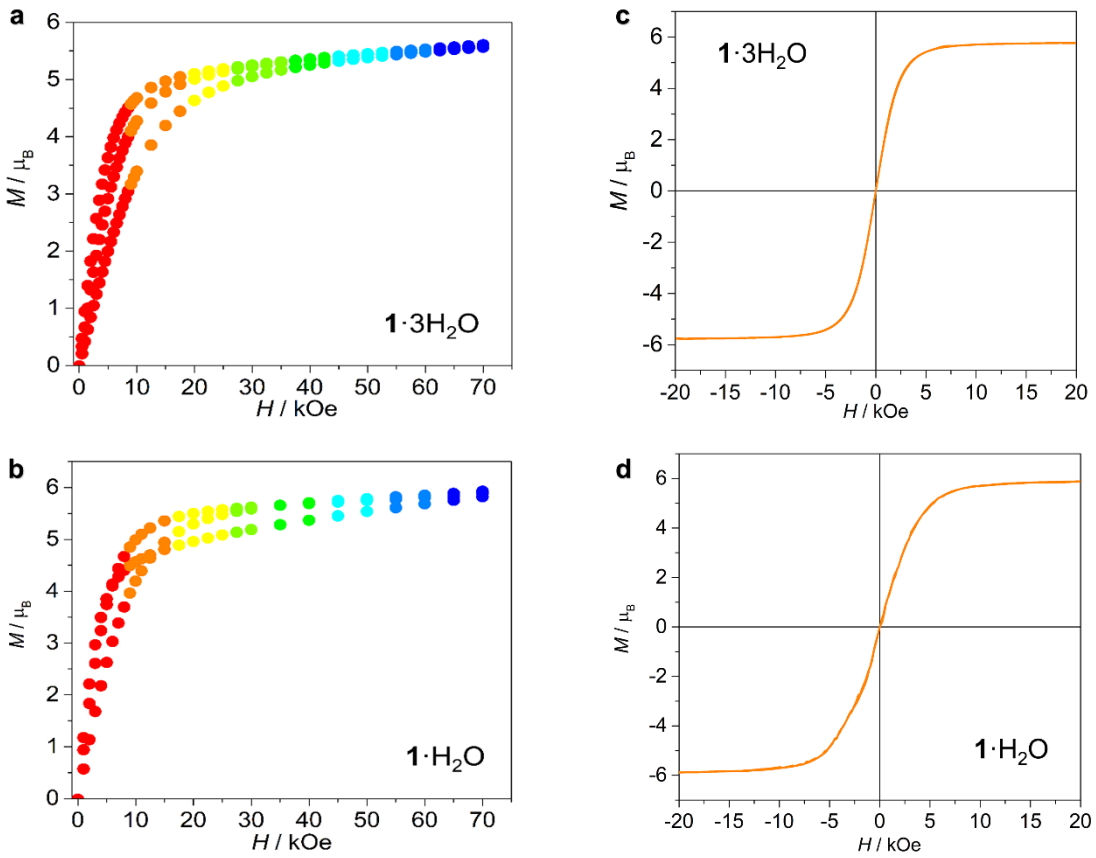

Figure S6. Magnetization versus applied magnetic fields curves for **1**·3H_2O (a) and **1**·H_2O (b) collected at 2, 3, and 5 K. Magnetization versus field hysteresis measurements for **1**·3H_2O (c) and **1**·H_2O (d) collected at 1.8 K with a field sweep rate of 0.03 T s^{-1}.

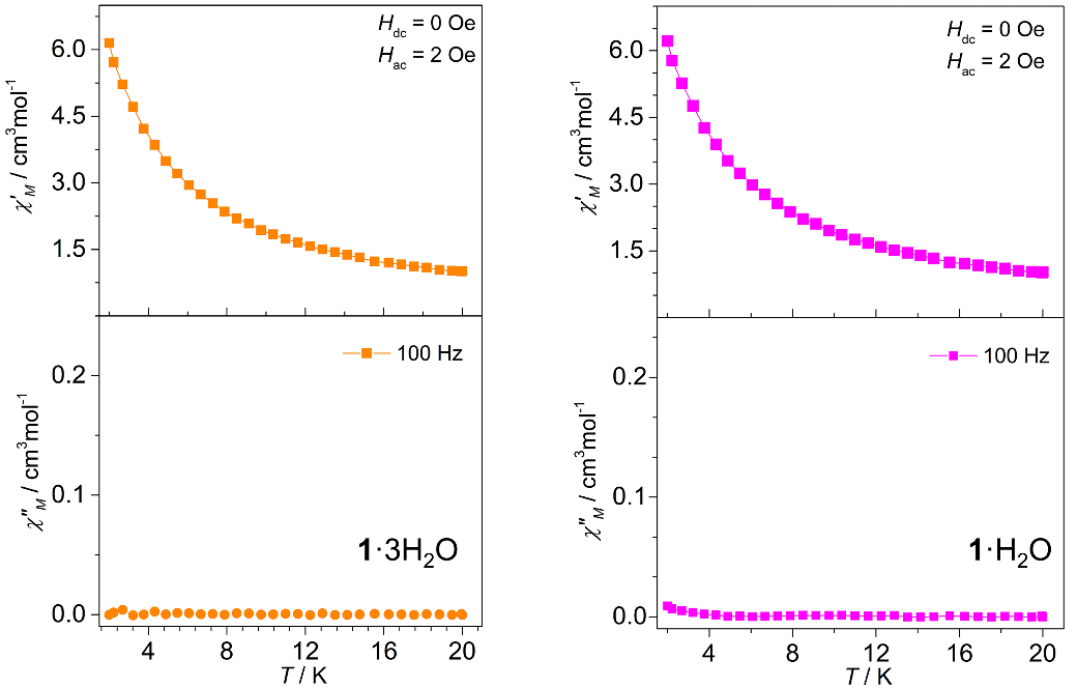

Figure S7. Temperature dependence of the in-phase (χ') and out-of-phase (χ'') ac susceptibilities measured under zero dc field using a 100 Hz frequency for **1**·3H$_2$O (left) and **1**·H$_2$O (right).

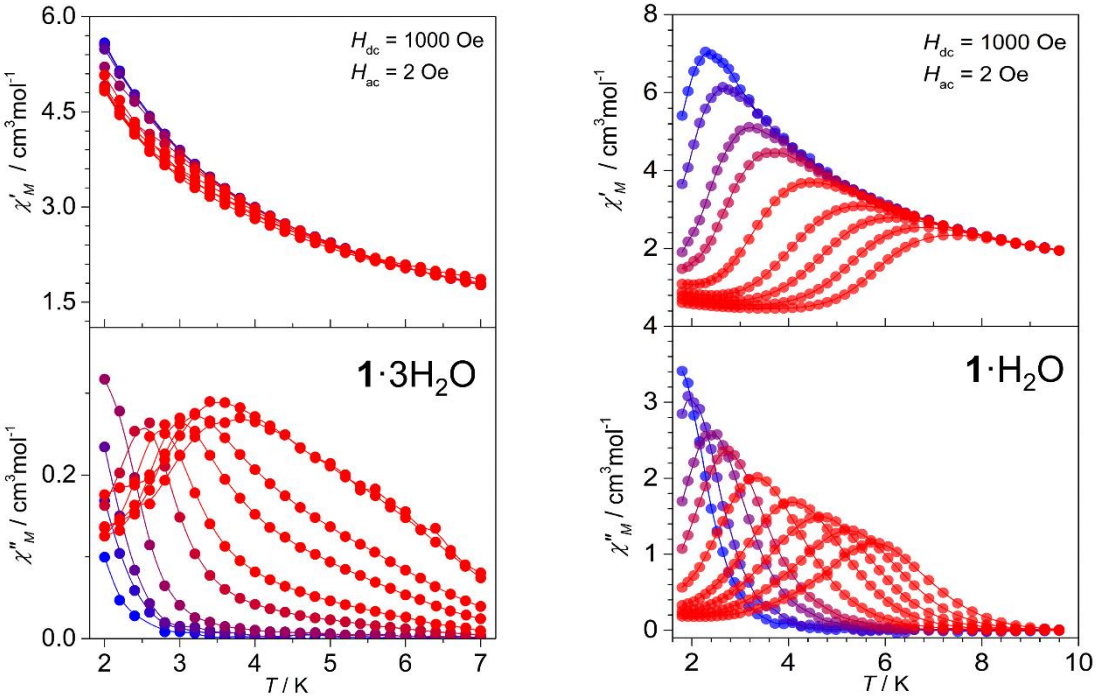

Figure S8. Temperature dependence of the in-phase (χ') and out-of-phase (χ'') part of the ac susceptibilities measured under 1 kOe dc field for **1**·3H$_2$O (left) and **1**·H$_2$O (right).

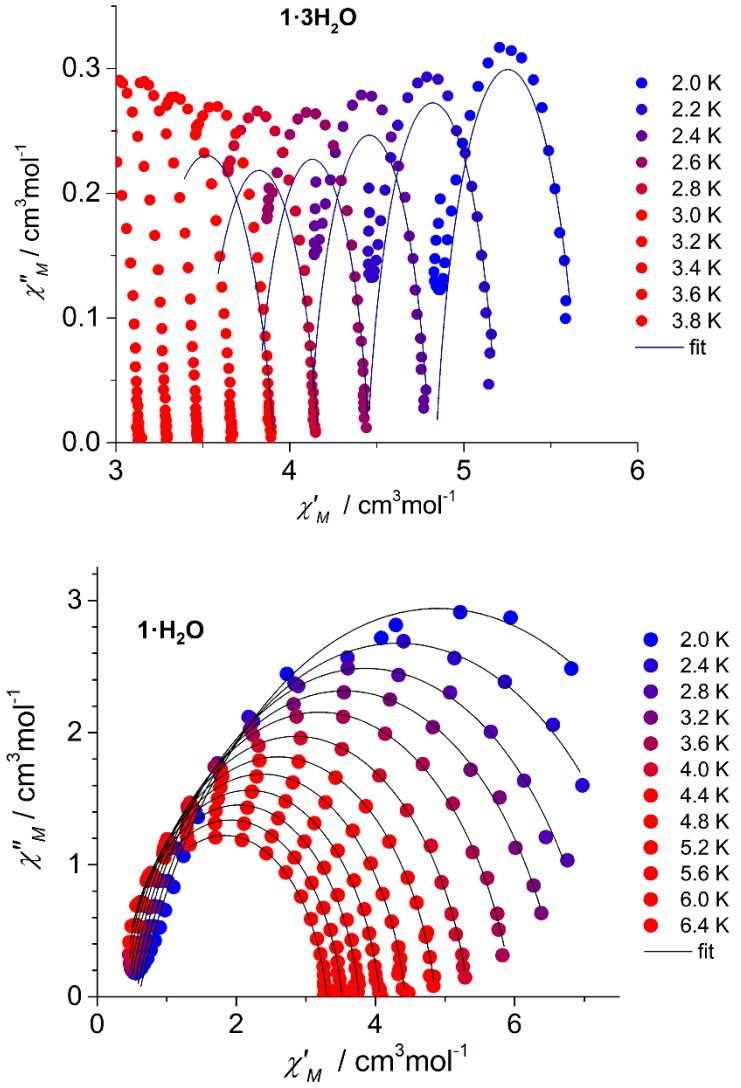

Figure S9. Cole-Cole plots for **1**·3H2O (up) and **1**·H2O (down) under 1 kOe dc field.

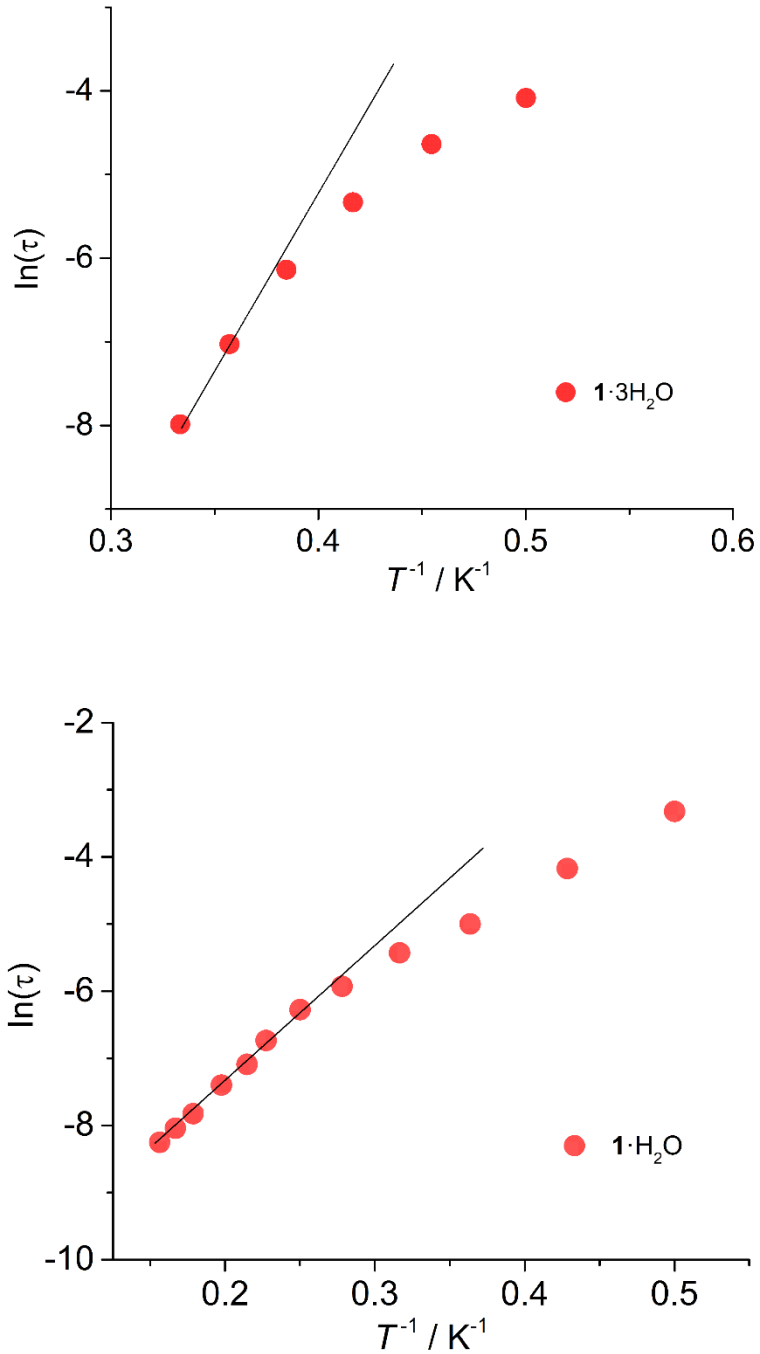

Figure S10. Natural logarithm of the relaxation time as a function of temperature for **1**·3H_2O (up) and **1**·H_2O (down). The black straight line represents the fit via the Orbach process.

Table S6. Relaxation fitting parameters from the least-square fitting of the Cole-Cole plots of **1**·3H_2O under 1 kOe dc filed according to the generalized Debye model.

T / K	τ / s	χ_S / $cm^3mol^{-1}K$	χ_T / $cm^3mol^{-1}K$	α
1.99992	0.0168	4.84107	5.66499	0.20011
2.19998	0.00969	4.44761	5.19439	0.19736
2.39999	0.00483	4.11363	4.80098	0.20786
2.59996	0.00216	3.80259	4.45673	0.22694
2.80009	8.86118E-4	3.48146	4.16673	0.2776
2.99989	3.39651E-4	3.13061	3.91111	0.32131

Table S7. Relaxation fitting parameters from the least-square fitting of the Cole-Cole plots of **1**·H_2O under 1 kOe dc filed according to the generalized Debye model.

T / K	τ / s	χ_S / $cm^3mol^{-1}K$	χ_T / $cm^3mol^{-1}K$	α
1.99993	0.03602	0.6503	9.83789	0.24958
2.39996	0.0154	0.57885	8.55246	0.22381
2.79997	0.00673	0.52201	7.63228	0.20474
3.19974	0.00439	0.47459	6.94289	0.18905
3.59014	0.00267	0.43779	6.30616	0.1707
4.00099	0.00188	0.40479	5.60678	0.14611
4.39996	0.00119	0.35093	5.06421	0.14243
4.80009	8.32987E-4	0.32515	4.62531	0.1312
5.19986	6.11578E-4	0.30698	4.24401	0.12207
5.59804	3.9991E-4	0.29592	3.91975	0.1168
5.99938	3.21663E-4	0.29625	3.64638	0.11619
6.40003	2.6098E-4	0.32692	3.40975	0.11716

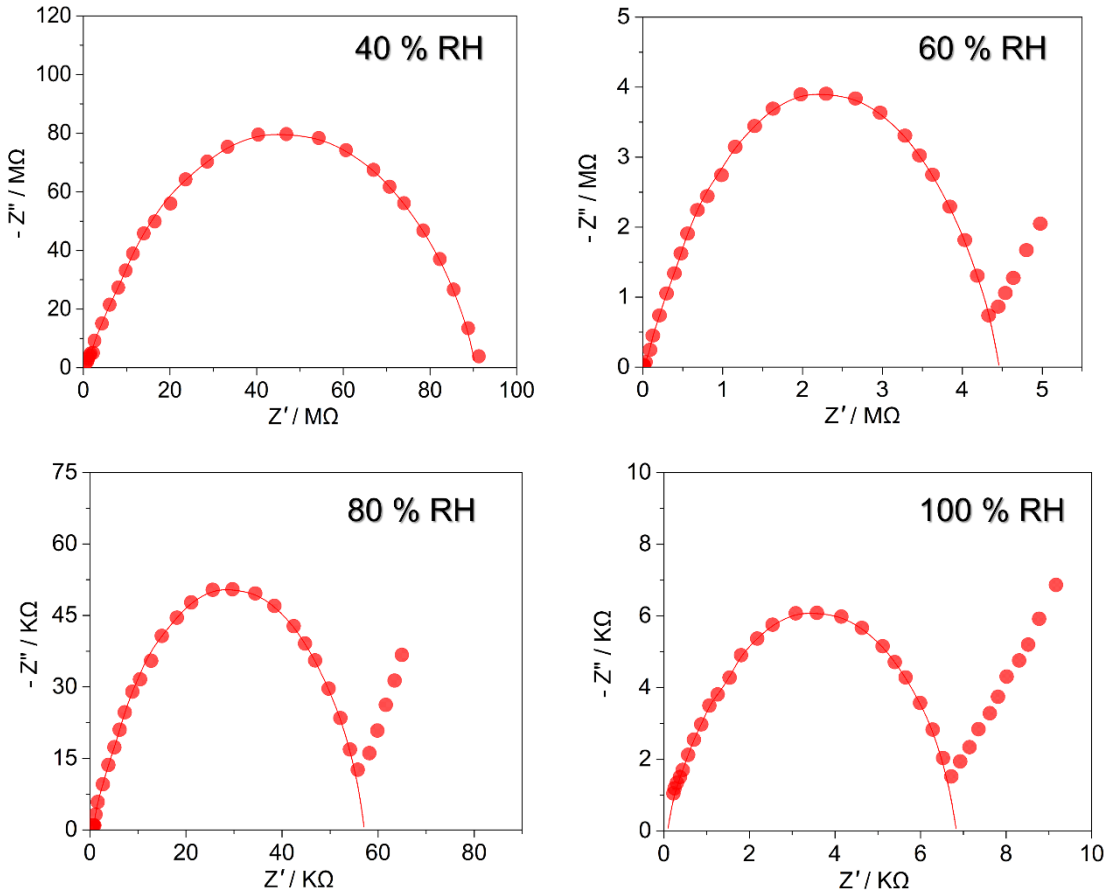

Figure S11. Nyquist plots of **1**·3H_2O measured at 25 ℃ under different relative humidity in the 40-100% range. Solid red lines represent fitted semicircles, and the extracted values of conductivity were listed in Table S8.

Table S8. The conductivity of **1**·3H_2O extracted from impedance spectra gathered at 25 ℃ under variable indicated relative humidity.

RH%	σ / S cm^{-1}
40	2.1×10^{-9}
60	3.5×10^{-7}
80	1.7×10^{-5}
100	1.1×10^{-4}

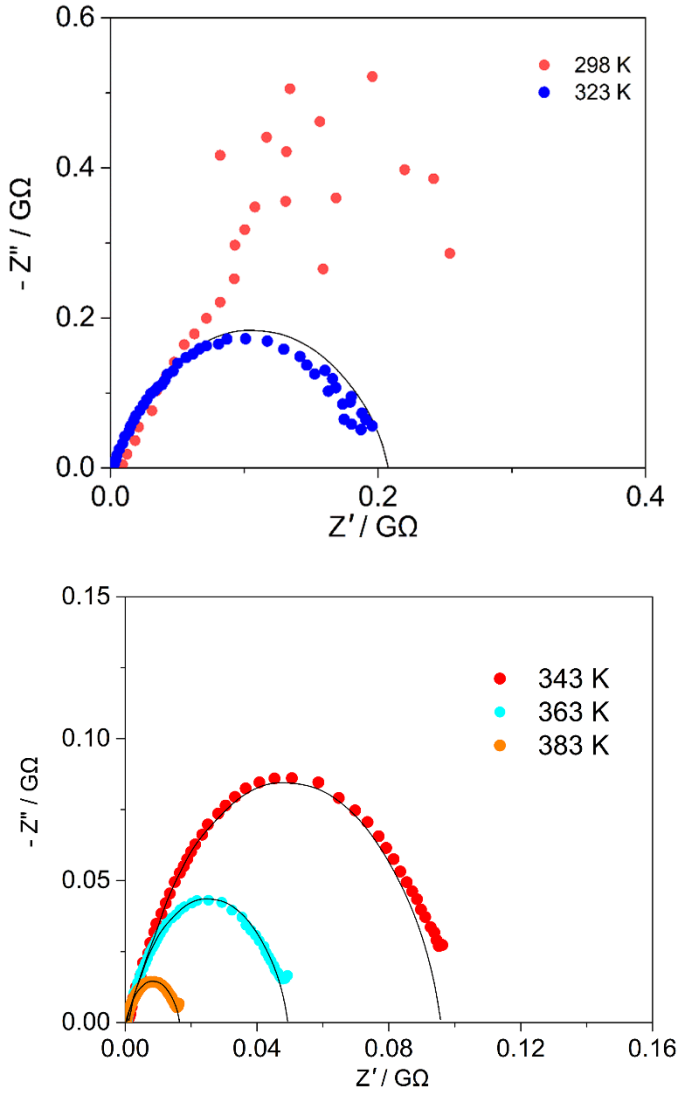

Figure S12. Nyquist plots of **1**·H_2O measured at different temperature (298 – 383 K) under 40% relative humidity. Solid red lines represent fitted semicircles.

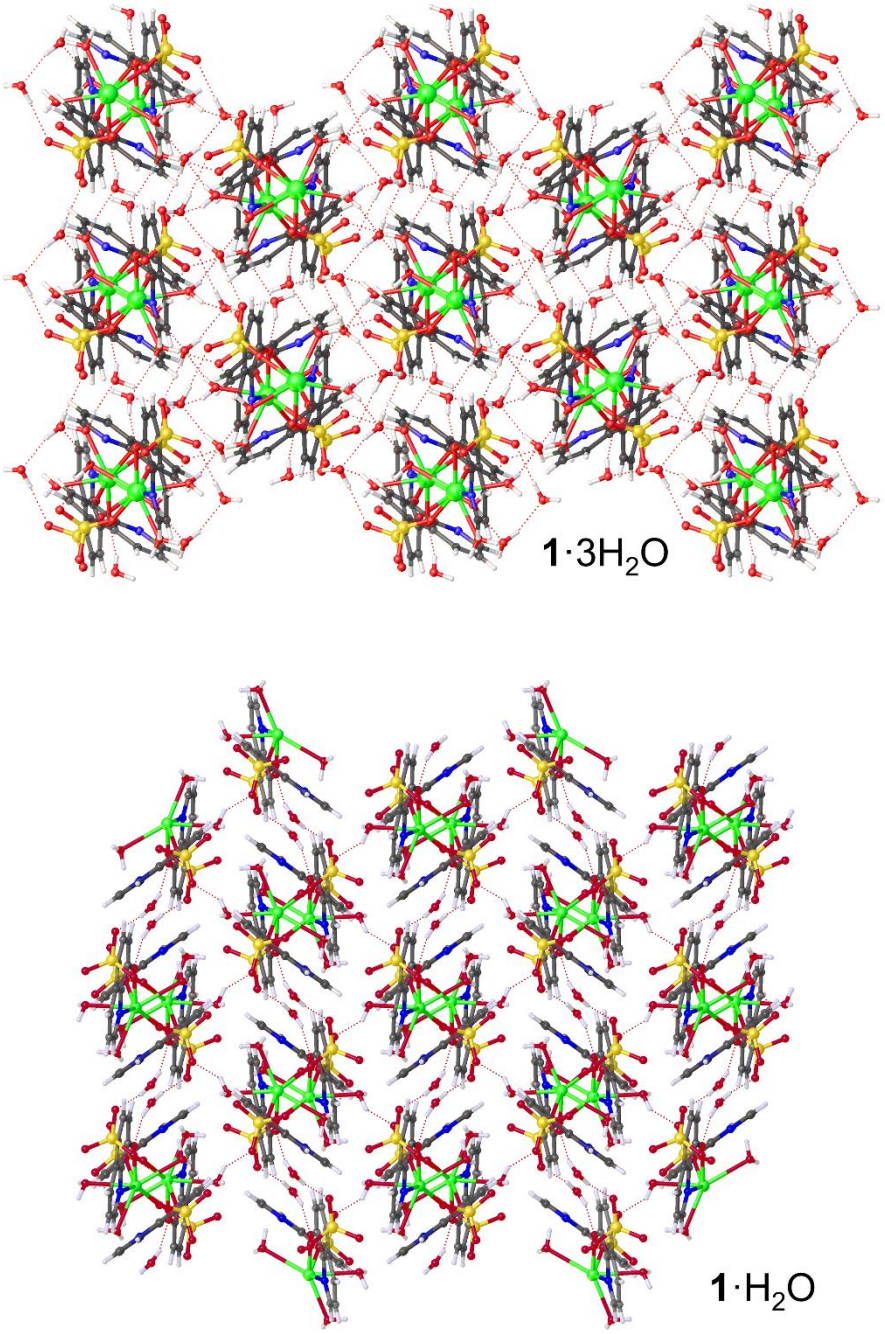

Figure S13. Hydrogen-bonded supramolecular 3D structures of **1**·3H$_2$O (up) and **1**·H$_2$O (down).

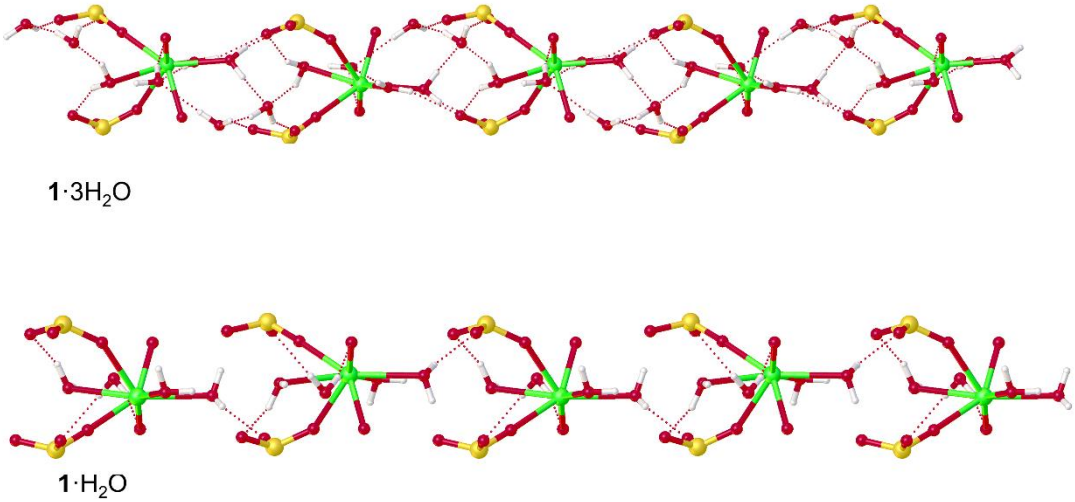

Figure S14. 1D hydrogen-bonded H_2O chains in **1**·3H_2O (up) and **1**·H_2O (down) along *b* axis direction.

Computational Details

All the DFT calculations were performed using ORCA 4.2.1 code.[S5] The position of hydrogens was optimized for the prepared model using BP86 level of theory and SV basis set for all atoms. Dispersion corrections have been taken care of by incorporating Grimme's atom-pairwise dispersion correction approach as implemented in ORCA.[S6,S7,S8]

All the multireference calculations were performed on the model of **1**·3H_2O and **1**·H_2O using Open MOLCAS code.[S9,S10] The spin-Hamiltonian parameters were calculated using a complete active space self-consistent field (CASSCF) method.[S11] Here, we have employed the ANO-RCC-VDZP type basis set for the paramagnetic ion Dy^{III}, while the ANO-RCC-VDZ type basis set was used for the rest of the atoms.[S12,S13] The details of the basis set and contraction scheme are provided in the Table S15. To speed up the calculations, the two-electron integrals were computed using the resolution of identity Cholesky decomposition (RICD) approximation. For CASSCF calculations, the active space comprises CAS(*9*,7).Using this active spaces, we have computed 21 sextets for Dy^{III} ions in both **1**·3H_2O and **1**·H_2O. Subsequently, these states were mixed in the spin–orbit restricted active space state interaction (SO-RASSI) module to compute the spin–orbit states.[S14] The calculated spin-free energies and SOC states for **1**·3H_2O and **1**·H_2O are reported in Tables S9 and S10. The computed spin–orbit coupled (SOC) states were used to calculate the *g*-values, crystal field parameters, transition magnetic moments, magnetic susceptibility, and magnetization of Dy^{III} with the SINGLE_ANISO module[S15] as implemented in MOLCAS.

Table S9. RASSI-SO computed low-lying 21 spin-free sextet states and the spin-orbit coupled (Kramer doublets) for Dy in complex **1·3H$_2$O** at 300K. All the values are reported here in cm^{-1}.

Complex **1.3H$_2$O**		
SPIN-FREE STATES	**SPIN-ORBIT STATES**	
0.0	0.0	9862.8
14.9	157.5	9937.3
205.7	235.7	10012.6
238.6	303.5	11099.0
305.6	335.1	11291.7
367.2	407.7	11430.0
402.7	478.3	11881.6
484.7	608.7	11909.0
531.2	3075.7	11938.9
653.7	3190.2	11955.6
666.1	3264.7	11990.7
7642.5	3323.7	13673.1
7665.2	3368.2	13696.3
7760.9	3417.1	13756.4
7790.9	3489.5	13769.4
7823.4	5707.7	15087.6
7887.3	5805.3	15112.4
7905.2	5888.6	15149.3
34622.9	5931.4	16108.6
35103.1	5973.7	16121.0
35210.8	6043.0	16714.3
	7925.6	38764.6
	8017.8	38814.7
	8099.6	38905.6
	8140.3	39105.4
	8215.0	40164.1
	9653.4	40363.2
	9672.7	40494.7
	9700.7	41311.3
	9734.8	41383.5
	9756.4	
	9779.1	
	9816.5	

Table S10. RASSI-SO computed low-lying 21 spin-free sextet states and the spin-orbit coupled (Kramer doublets) for Dy in complex **1**·H_2O at 400K. All the values are reported here in cm^{-1}.

Complex **1**·H_2O		
SPIN-FREE STATES	**SPIN-ORBIT STATES**	
0.0	0.0	9810.8
25.0	140.2	9871.5
170.8	184.8	9961.4
241.0	245.5	11085.1
291.3	297.7	11225.4
339.9	342.0	11373.0
366.8	423.0	11838.6
447.2	549.0	11871.4
464.3	3082.8	11883.8
620.1	3169.0	11906.6
628.7	3212.7	11939.6
7598.2	3254.9	13623.4
7638.0	3313.8	13647.1
7754.2	3358.8	13707.2
7783.5	3431.6	13728.0
7798.1	5717.8	15035.4
7847.0	5769.5	15062.8
7860.7	5820.7	15107.0
34710.0	5864.3	16060.3
34921.7	5917.3	16073.8
35202.8	5995.5	16664.2
	7927.7	38736.7
	7967.7	38818.8
	8024.9	38883.0
	8083.9	38988.3
	8171.0	40136.0
	9608.6	40258.3
	9639.6	40437.9
	9670.1	41257.0
	9689.6	41311.5
	9718.2	
	9743.0	
	9752.8	

Table S11. SINGLE_ANISO computed g-tensors, the angle of deviation from ground state g_{zz} orientation and relative energies of eight low lying Kramers doublets for **1**·3H$_2$O and **1**·H$_2$O.

Complex **1**·3H$_2$O					Complex **1**·H$_2$O				
KDs Energy (cm^{-1})	g_{xx}	g_{yy}	g_{zz}	θ (° angle)	KDs Energy (cm^{-1})	g_{xx}	g_{yy}	g_{zz}	θ (° angle)
0.0	0.0142	0.0179	19.7880	0.0	0.0	0.0303	0.0542	19.6981	0.0
157.5	0.0833	0.1271	17.4577	160.0	140.2	1.6394	4.3021	13.9906	136.4
235.7	0.2271	0.5059	15.0220	146.8	184.8	0.7015	4.7669	8.8613	37.3
303.5	3.3806	6.6750	10.4133	115.9	245.5	2.9874	5.8806	9.8383	100.7
335.1	1.0096	3.1108	9.5208	69.5	297.7	0.5022	2.2905	12.8331	92.1
407.7	1.8340	2.2233	14.4210	71.5	342.0	0.8073	1.3927	16.1265	107.6
478.3	0.3474	0.6198	18.4471	75.0	423.0	0.0209	0.0587	18.0133	81.8
608.7	0.0265	0.0508	19.6533	65.5	549.0	0.0011	0.0040	19.4819	58.2

Table S12. SINGLE_ANISO computed crystal field parameters for **1**·3H$_2$O and **1**·H$_2$O.

k	**q**	B_k^q	
		Complex 1.3H$_2$O	**Complex 1.H$_2$O**
2	-2	-1.21E+00	3.26E+00
	-1	4.05E+00	-7.19E+00
	0	-5.30E+00	-3.31E+00
	1	-1.10E+01	-6.39E+00
	2	4.63E-01	-3.53E+00
4	-4	4.92E-02	3.56E-02
	-3	1.64E-01	-2.95E-01
	-2	-4.08E-02	1.39E-01
	-1	-4.72E-02	2.14E-02
	0	-2.82E-02	-3.07E-02
	1	1.34E-01	-1.69E-01
	2	-7.57E-02	7.76E-02
	3	4.12E-01	1.11E-01
	4	-7.45E-02	-5.40E-02

6	-6	-4.28E-04	6.33E-04
	-5	-3.90E-03	-5.62E-03
	-4	2.61E-03	2.07E-03
	-3	4.30E-03	-9.11E-03
	-2	3.02E-03	-7.67E-04
	-1	1.69E-03	-7.90E-04
	0	-2.94E-05	-1.11E-04
	1	1.46E-03	2.04E-03
	2	3.14E-03	-2.48E-04
	3	3.23E-03	5.13E-03
	4	-4.29E-03	-3.47E-03
	5	2.21E-03	-4.19E-03
	6	3.03E-03	-2.32E-03

Table S13. SINGLE_ANISO computed wave function decomposition analysis for Dy centre in complex **1**·3H_2O. The major dominating values are kept in bold.

±mJ	*wave function decomposition analysis of complex 1*
KD1	**97.7% |±15/2⟩**+1.0 % |±9/2⟩ + 0.7% |±7/2⟩
KD2	**81.7% |±13/2⟩** +11.5 % |±11/2⟩ + 3.5 % |±9/2⟩+2.1% |±5/2⟩
KD3	**35.0% |±11/2⟩** + 29.2 % |±9/2⟩ + 21.8 % |±7/2⟩ +9.4 % |±13/2⟩+1.4% |±15/2⟩
KD4	**38.0% |±5/2⟩+** 20.3% |±7/2⟩ + 16.3% |±11/2⟩+12.2% |±1/2⟩+7.7% |±3/2⟩+4.2% |±13/2⟩
KD5	**37.6% |±3/2⟩** + 18.7% |±11/2⟩+14.3% |±9/2⟩+12.7%|±1/2⟩+11.0%|±5/2⟩ +4.1% |±7/2⟩
KD6	**33.3% |±1/2⟩ +** 25.6 % |±9/2⟩+ 14.9% |±3/2⟩ + 10.0 % |±11/2⟩ +8.6 % |±7/2⟩+ 7.3% |±5/2⟩
KD7	**36.0 % |±1/2⟩** + 21.1% |±3/2⟩ +19.4% |±7/2⟩ + 12.7% |±5/2⟩ +9.5 %|±9/2⟩
KD8	**27.7 % |±5/2⟩** +24.4% |±7/2⟩+17.5 % |±3/2⟩+ 15.2% |±9/2⟩ +7.5%|±11/2⟩ +5.4% |±1/2⟩

Table S14. SINGLE_ANISO computed wave function decomposition analysis for Dy centre in complex **1**·H_2O. The major dominating values are kept in bold.

±mJ	*wave function decomposition analysis of complex 2*
KD1	**96.7% |±15/2⟩**+ 1.1 % ±|9/2⟩+1.0% |±11/2⟩
KD2	**48.0% |±13/2⟩** +12.1 % |±3/2⟩ + 11.4 % |±1/2⟩+9.9% |±5/2⟩+8.3% |±9/2⟩+7.9% |±7/2⟩
KD3	**37.6% |±13/2⟩** + 18.5 % |±1/2⟩ + 14.0 % |±11/2⟩ +12.1% |±3/2⟩ + 8.6 % |±5/2⟩+6.5% |±7/2⟩

KD4	**35.0% |±11/2⟩** +15.1 % |±3/2⟩ + 12.7% |±7/2⟩ + 12.6% |±9/2⟩ + 12.6 % |±5/2⟩ **+ 7.4 %** |±1/2⟩
KD5	**22.3% |±11/2⟩** + 22.1% |±9/2⟩ + 18.2 % |±1/2⟩ +14.3 % |±5/2⟩ + 14.0% |±7/2⟩ + 7.9 % |±3/2⟩
KD6	**26.6% |±7/2⟩** + 23.6 % |±5/2⟩+ 22.8% |±9/2⟩ + 15.6 % |±3/2⟩ + 6.9 % |±11/2⟩
KD7	**39.5 % |±1/2⟩** + 29.3 % |±3/2⟩ + 11.1 % |±5/2⟩ + 8.7 % |±9/2⟩ + 6.2 % |±7/2⟩
KD8	**25.7% |±7/2⟩**+22.2 % |±9/2⟩+ 19.6 % |±5/2⟩ + 15.2 % |±11/2⟩ + 8.0 % |±3/2⟩ + 6.8 % |±13/2⟩

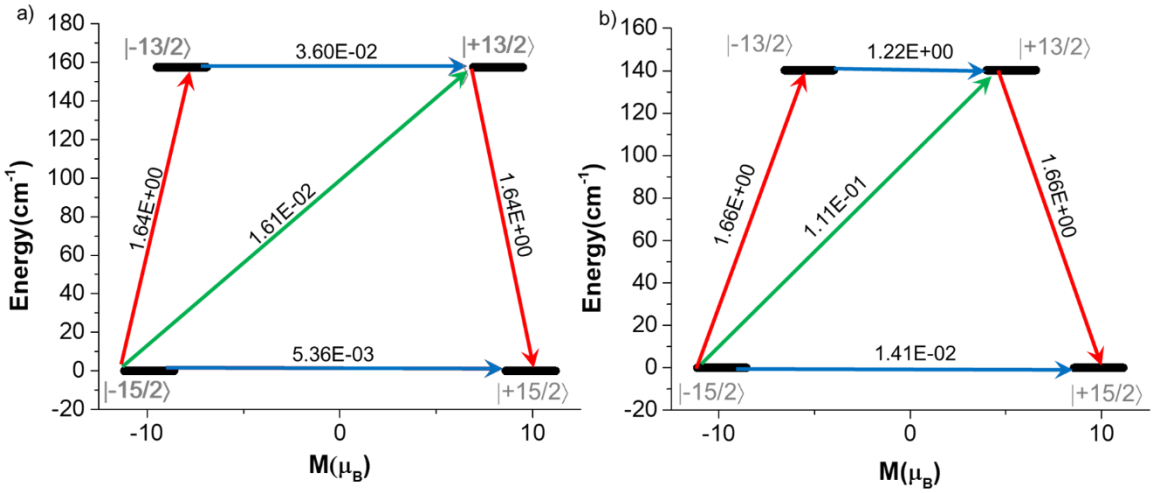

Figure S15. Ab initio computed magnetic relaxation pathway of the a) **1**·3H_2O and b) **1**·H_2O. The grey line indicates the KDs as a function of magnetic moments. The blue, red and green lines represent thermal, QTM, and possible Orbach relaxations.

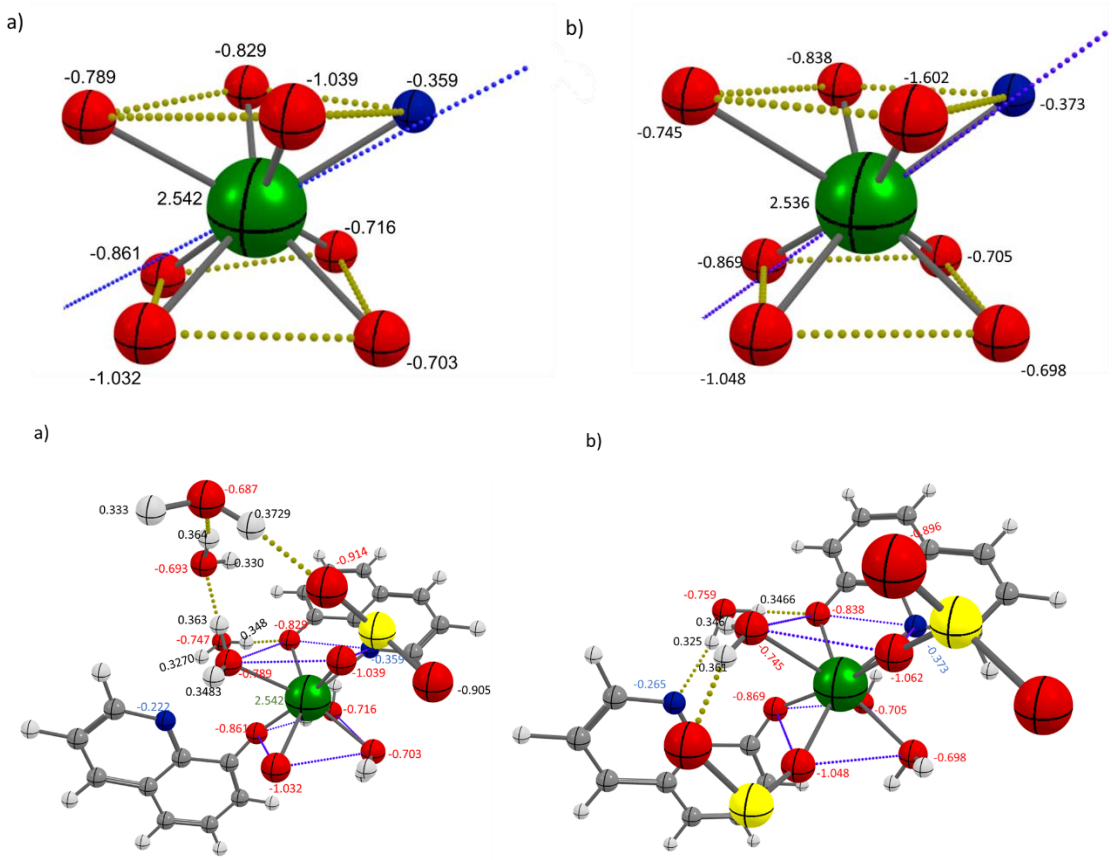

Figure S16. LoProp charge for the two Dy centers in a) Complex **1**·3H_2O and b) Complex **1**·H_2O. (in core as well as in the vicinity of neighboring water molecules) Color code: Dy (Green); N (blue), O (red), C (grey), H(white).

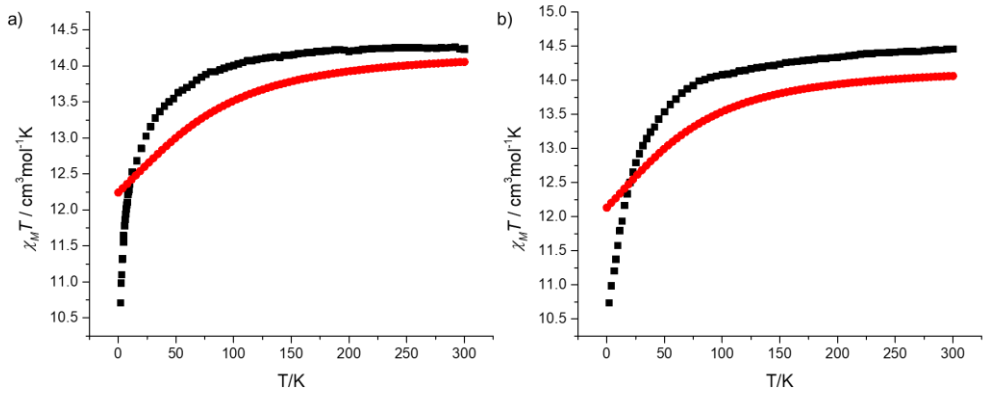

Figure S17. SINGLE_ANISO fitting for χ_MT vs T for a) Complex **1**·3H$_2$O and b) Complex **1**·H$_2$O. Red (calculated); black (experimental).

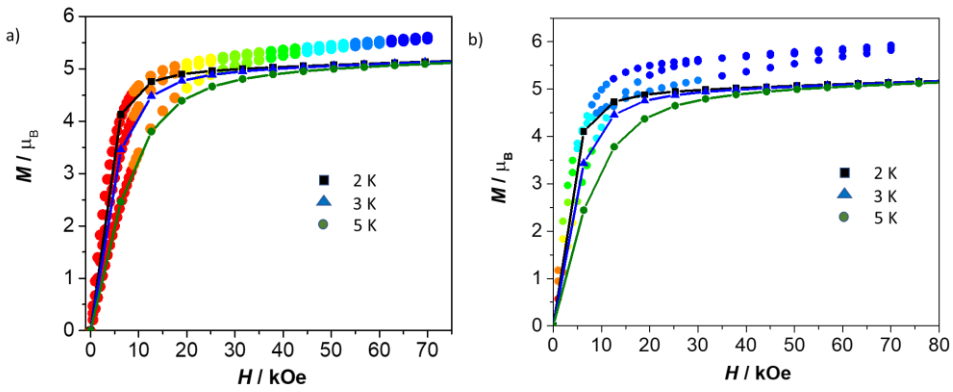

Figure S18. Experimental versus Calculated M vs H plot at different temperatures (2K, 3K, 5K) for a) Complex **1**·3H$_2$O and b) Complex **1**·H$_2$O.

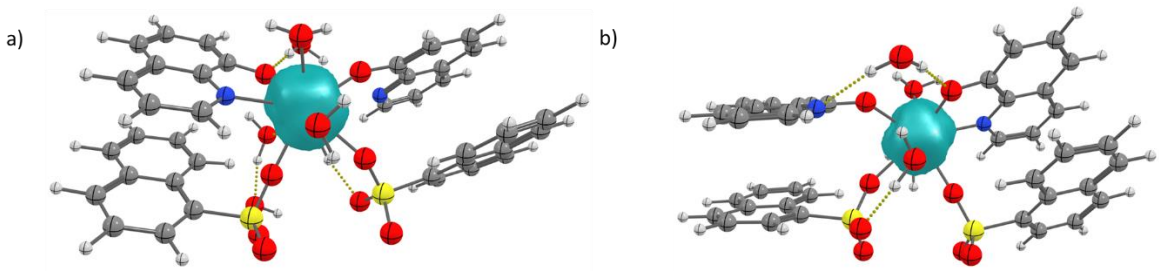

Figure S19. DFT calculated beta spin density plot for a) Complex **1**·3H$_2$O b) Complex **1**·H$_2$O at iso value 0.000433 e$^-$/bohr^3. Color code: N (blue), O (red), S (yellow), C (grey), H(white).

Table S15. Basis functions used in *ab initio* CASSCF calculations using OpenMolcas code.

Atoms	**ANO-RCC basis functions**
H	2s
C	3s2p
N, O	3s2p
Dy	7s6p4d2f1g.

Table S16. Hydrogen optimized coordinates for mononuclear model of **1**·3H_2O and **1**·H_2O.

Complex **1**·3H_2O			
Dy	0.00000	0.00000	0.00000
S	1.62180	-1.88957	2.77025
S	1.12090	2.33416	2.75164
O	-0.53710	-2.09181	-0.55876
O	-1.40416	-0.74229	1.91489
O	-2.15480	0.65326	-0.36400
O	2.24366	0.39401	-0.66249
O	0.00000	0.00000	-2.37216
O	1.37611	-1.37104	1.42727
O	0.61336	1.44096	1.71808
O	-4.07310	-1.27016	-0.32734
O	-3.58572	0.49337	2.84498
O	-2.15137	1.57832	4.85472
O	0.57477	-1.53028	3.71116
O	2.95212	-1.52739	3.22933
O	0.49260	2.06291	4.02363
O	2.56647	2.33420	2.80122
N	-1.94043	-3.46484	1.25911
N	-0.18820	2.38219	-0.86481
C	-0.42911	-3.37921	-0.57758
C	-2.12207	-6.17952	1.27124
C	0.58173	4.56075	-1.46110
C	-1.22038	-4.15827	0.33125
C	-3.79732	2.17504	-1.16147

C	-3.14085	4.42788	-1.79009
C	-2.70900	-4.04924	2.15981
C	-1.77303	4.09992	-1.55751
C	-4.10703	3.47114	-1.60673
C	0.79444	3.24480	-1.04313
C	0.40078	-4.10538	-1.42272
C	-1.46653	2.78651	-1.11939
C	-0.45142	-6.24131	-0.61994
C	-1.27523	-5.56751	0.32712
C	-2.83783	-5.42962	2.17082
C	-0.69066	4.98816	-1.70529
C	0.36493	-5.50537	-1.44004
C	-2.49628	1.81353	-0.87676
C	3.07627	-6.42284	0.74374
C	1.56496	-6.50848	2.58043
C	3.25791	-3.70817	0.73161
C	2.35622	-5.72942	1.67160
C	3.84484	-5.83845	-0.15696
C	0.73507	-5.78231	3.42557
C	1.58726	-3.64638	2.62279
C	2.41107	-4.32018	1.67573
C	3.97367	-4.45807	-0.16797
C	0.77091	-4.38232	3.44289
C	-2.30511	6.01008	1.33304
C	-3.07504	3.83151	1.92933
C	1.30400	6.21722	1.62971
C	0.64754	3.96439	2.25833
C	-0.72028	4.29234	2.02574
C	1.61372	4.92112	2.07496
C	-3.28775	5.14747	1.51137
C	-1.02678	5.60575	1.58763
C	-1.80265	3.40411	2.17353
C	0.00297	6.57873	1.34499
H	-2.28366	-0.29428	2.20140
H	-0.79002	-0.95651	2.69194
H	2.58492	0.10256	0.24616
H	2.43148	-0.31710	-1.33469
H	-0.40963	-0.93223	-2.27258
H	-0.72038	0.66488	-2.55596
H	-2.19655	-7.28151	1.27580
H	1.44361	5.23725	-1.55997
H	-4.58781	1.42577	-0.99357
H	-3.24221	-3.39161	2.87125
H	-5.16520	3.72116	-1.79610

H	1.80719	2.86701	-0.82909
H	1.08382	-3.55849	-2.09367
H	-3.49874	-5.92572	2.90360
H	-0.89225	6.02713	-2.01716
H	1.03450	-6.03349	-2.14187
H	-3.33764	-0.57840	-0.40656
H	-3.65569	-1.95630	0.26894
H	-3.13437	1.07137	3.58055
H	-3.92336	1.01889	2.07564
H	-1.20351	1.84386	4.54736
H	-2.02918	0.76633	5.41626
H	3.32773	-2.61092	0.73060
H	4.40052	-6.43992	-0.89745
H	0.04604	-6.29863	4.11508
H	4.62936	-3.95982	-0.90115
H	0.11180	-3.82343	4.12781
H	-3.92510	3.14487	2.05003
H	2.12907	6.93661	1.48604
H	2.65873	4.62715	2.27096
H	-4.33045	5.45104	1.30709
H	-1.62162	2.35292	2.43788
H	-0.44873	-7.34444	-0.65586
H	-3.39604	5.44996	-2.11475
H	-0.26958	7.58046	0.97802
H	-2.49261	7.03659	0.97957
H	2.99084	-7.52440	0.75098
H	1.57582	-7.60688	2.53095

Complex **1**·H_2O

Dy	0.00000	0.00000	0.00000
S	-2.15260	-1.24684	2.78530
S	-0.66970	2.59986	2.46540
O	1.68822	-1.45913	-0.16553
O	1.60397	1.44205	-0.57850
O	-2.16716	0.61961	-0.79583
O	0.00000	0.00000	-2.44180
O	1.42817	0.00000	2.18657
O	-0.53481	1.94871	1.18656
O	-1.29054	-0.80780	1.69904
O	4.09456	-0.29724	0.55905
O	-1.51308	-1.06312	4.06829
O	-3.46538	-0.66292	2.70610

O	0.20429	2.09589	3.48594
O	-2.04176	2.63276	2.86793
N	-0.75542	-2.30995	-0.70905
N	3.33843	2.51653	1.12935
C	0.25538	-3.24193	-0.71761
C	4.48394	4.32731	2.09494
C	-1.98021	-2.74917	-0.92944
C	0.02460	-4.61501	-0.94014
C	2.40170	5.47984	-0.79045
C	1.15723	-5.49006	-0.91656
C	3.94241	5.17607	1.18255
C	3.04188	4.69763	0.19955
C	2.60660	-3.61743	-0.47069
C	1.56283	-2.72919	-0.44644
C	-2.29733	-4.08197	-1.14056
C	-1.32522	-5.00549	-1.15955
C	1.45870	4.91087	-1.58704
C	2.73585	3.33138	0.21751
C	1.14324	3.57406	-1.51747
C	2.40138	-4.97739	-0.70705
C	4.17080	2.99784	2.04819
C	1.79264	2.72329	-0.66197
C	-0.45660	-6.16059	2.32960
C	-1.46740	-5.22860	2.33817
C	0.76820	-5.72137	2.54999
C	-1.23661	-3.85552	2.56070
C	-2.36924	-2.98048	2.53712
C	-3.81861	-4.85311	2.09124
C	-2.77484	-5.74135	2.06700
C	1.08532	-4.38856	2.76112
C	0.11321	-3.46504	2.78010
C	-3.61339	-3.49314	2.32761
C	-1.14730	7.25386	0.26912
C	-2.29282	5.44308	-0.69647
C	-0.21057	4.29055	2.18893
C	-1.75128	4.59432	0.21592
C	-0.85075	5.07277	1.19892
C	0.73243	4.85952	2.98551
C	-0.54472	6.43901	1.18096
C	1.04789	6.19634	2.91594
C	-1.97967	6.77255	-0.64972
C	0.39849	7.04711	2.06044
H	-2.02278	1.51371	-1.21024
H	-2.53688	0.74406	0.13597

H	0.09242	-0.98630	-2.56364
H	0.91538	0.42377	-2.32148
H	1.08990	0.74552	2.79317
H	2.36393	0.15784	1.86092
H	5.17424	4.70633	2.86779
H	-2.77060	-1.98047	-0.91100
H	4.18478	6.25274	1.19131
H	3.61629	-3.23119	-0.25943
H	-3.35385	-4.35602	-1.28122
H	-1.54646	-6.07502	-1.31506
H	0.91458	5.54491	-2.30858
H	0.35565	3.15566	-2.16700
H	3.27510	-5.65138	-0.69321
H	4.60927	2.26248	2.74547
H	3.83969	0.68411	0.58715
H	3.26639	-0.76638	0.20984
H	1.60904	-6.44142	2.54288
H	-4.85071	-5.20398	1.90977
H	2.13469	-4.08935	2.90593
H	0.34789	-2.39823	2.93526
H	-4.45925	-2.78467	2.32918
H	-2.98571	5.05846	-1.46343
H	-1.98669	3.52062	0.21602
H	1.23978	4.20375	3.71338
H	1.82774	6.58583	3.59412
H	-2.43490	7.45719	-1.38805
H	0.60361	8.12602	1.99923
H	-0.90471	8.33084	0.28398
H	2.61713	6.56035	-0.84872
H	-2.91219	-6.81690	1.87408
H	-0.68196	-7.22229	2.14355
H	0.99449	-6.56922	-1.07309

Table S17. The possible hydrogen bonds in **1**·3H_2O at 150 K calculated by PLATON.

D-H...A	d(D- H)	d(H...A)	d(D...A)	＜(DHA)
O(1)-H(1A)...O(6)	0.84	1.87	2.6914	165
O(1)-H(1B)...O(11)	0.85	2.23	2.9820	147
O(2)-H(2A)...O(3)	0.85	1.88	2.6771	156
O(2)-H(2B)...O(14)	0.85	1.95	2.7338	154
O(3)-H(3A)...O(12)	0.85	1.97	2.8002	168
O(3)-H(3B)...O(1)	0.85	1.94	2.7826	169
O(5)-H(5A)...O(2)	0.85	1.87	2.6606	154
O(5)-H(5B)...O(9)	0.85	1.99	2.7730	152
O(7)-H(7B)...O(1)	0.85	1.90	2.7341	171
O(7)-H(7B)...O(9)	0.85	2.11	2.9153	159
O(8)-H(8A)...O(2)	0.85	1.85	2.6948	173
O(8)-H(8B)...O(11)	0.85	1.95	2.7569	159

Table S18. The possible hydrogen bonds in **1**·3H_2O at 300 K calculated by PLATON.

D-H...A	d(D- H)	d(H...A)	d(D...A)	＜(DHA)
O(1)-H(1A)...O(6)	0.85	1.88	2.7168	166
O(1)-H(1B)...O(11)	0.85	2.24	3.0482	142
O(2)-H(2A)...O(3)	0.85	1.89	2.6966	158
O(2)-H(2B)...O(14)	0.85	1.98	2.7427	150
O(3)-H(3A)...O(12)	0.85	2.00	2.8139	160
O(3)-H(3B)...O(1)	0.85	1.96	2.7826	171
O(5)-H(5A)...O(2)	0.85	1.88	2.8081	154
O(5)-H(5B)...O(9)	0.85	2.00	2.6740	154
O(7)-H(7B)...O(1)	0.85	1.91	2.7863	171
O(7)-H(7B)...O(9)	0.85	2.13	2.9529	164
O(8)-H(8A)...O(2)	0.85	1.89	2.7136	163
O(8)-H(8B)...O(11)	0.85	1.95	2.7603	159

Table S19. The possible hydrogen bonds in **1**·H_2O at 353 K calculated by PLATON.

D-H...A	d(D- H)	d(H...A)	d(D...A)	＜(DHA)
O(3)-H(3A)...O(10)	0.87	2.03	2.8692	163
O(3)-H(3B)...O(6)	0.87	2.13	2.9068	148
O(4)-H(4A)...O(9)	0.85	1.90	2.6836	152
O(4)-H(4B)...O(12)	0.85	2.24	2.9860	147
O(5)-H(5A)...O(7)	0.87	1.93	2.7495	157
O(5)-H(5B)...O(6)	0.87	2.41	3.2081	152
O(6)-H(6B)...O(1)	0.85	1.91	2.7596	174
O(6)-H(6B)...O(12)	0.85	2.12	2.9574	168

Table S20. The possible hydrogen bonds in **1**·H_2O at 400 K calculated by PLATON.

D-H...A	d(D- H)	d(H...A)	d(D...A)	＜(DHA)
O(3)-H(3A)...O(10)	0.86	2.33	2.8702	121
O(3)-H(3B)...O(6)	0.86	2.56	2.9966	113
O(3)-H(3B)...O(10)	0.86	2.56	2.8702	102
O(4)-H(4A)...O(9)	0.85	1.91	2.6643	147
O(4)-H(4B)...O(12)	0.85	2.28	3.0005	142
O(5)-H(5A)...O(7)	0.87	2.03	2.7533	140
O(5)-H(5B)...O(6)	0.87	2.33	3.1378	155
O(6)-H(6B)...O(1)	0.85	1.94	2.7685	165
O(6)-H(6B)...O(12)	0.85	2.12	2.9623	170

Reference

(1) SAINT Software Users Guide, version 7.0; Bruker Analytical Xray Systems: Madison, WI, **1999**.

(2) Sheldrick, G. M. SADABS, version 2.03; Bruker Analytical X-ray Systems: Madison, WI, **2000**.

(3) Sheldrick, G. M. SHELXTL, version 6.14; Bruker AXS, Inc.: Madison, WI, **2000−2003**.

(4) Dolomanov, O. V.; Bourhis, L. J.; Gildea, R. J.; Howard, J. A. K.; Puschmann, H. OLEX2: A Complete Structure Solution, Refinement and Analysis Program. *J. Appl. Crystallogr*. **2009**, 42 (2), 339−341.

(5) Neese, F. Software Update: The ORCA Program System, Version 4.0. Wiley Interdiscip. Rev. Comput. Mol. Sci. **2018**, 8, 1–6.

(6) Neese, F.; Wennmohs, F.; Becker, U.; Riplinger, C. The ORCA Quantum Chemistry Program Package. J. Chem. Phys. **2020**, 152.

(7) Grimme, S.; Antony, J.; Ehrlich, S.; Krieg, H. A Consistent and Accurate Ab Initio Parametrization of Density Functional Dispersion Correction (DFT-D) for the 94 Elements H-Pu. J. Chem. Phys. **2010**, 132.

(8) Grimme, S.; Ehrlich, S.; Lars, G. Effect of the Damping Function in Dispersion Corrected Density Functional Theory. J. Comput. Chem. **2011**, 32, 1456–1465.

(9) I. F. Galván , M. Vacher , A. Alavi , C. Angeli , F. Aquilante , J. Autschbach , J. J. Bao , S. I. Bokarev , N. A. Bogdanov , R. K. Carlson , L. F. Chibotaru , J. Creutzberg , N. Dattani , M. G. Delcey , S. S. Dong , A. Dreuw , L. Freitag , L. M. Frutos , L. Gagliardi , F. Gendron , A. Giussani , L. González , G. Grell , M. Guo , C. E. Hoyer , M. Johansson , S. Keller , S. Knecht , G. Kovačević , E. Källman , G. Li Manni , M. Lundberg , Y. Ma , S. Mai , J. P. Malhado , P. Å. Malmqvist , P. Marquetand , S. A. Mewes , J. Norell , M. Olivucci , M. Oppel , Q. M. Phung , K. Pierloot , F. Plasser , M. Reiher , A. M. Sand , I. Schapiro , P. Sharma , C. J. Stein , L. K. Sørensen , D. G. Truhlar , M. Ugandi , L. Ungur , A. Valentini , S. Vancoillie , V. Veryazov , O. Weser , T. A. Wesołowski , P.-O. Widmark , S. Wouters , A. Zech , J. P. Zobel and R. Lindh , OpenMolcas: From Source Code to Insight, *J. Chem. Theory Comput.*, 2019, **15** , 5925 —5964.

(10) F. Aquilante , J. Autschbach , A. Baiardi , S. Battaglia , V. A. Borin , L. F. Chibotaru , I. Conti , L. De Vico , M. Delcey , I. F. Galván , N. Ferré , L. Freitag , M. Garavelli , X. Gong , S. Knecht , E. D. Larsson , R. Lindh , M. Lundberg , P. Å. Malmqvist , A. Nenov , J. Norell , M. Odelius , M. Olivucci , T. B. Pedersen , L. Pedraza-González , Q. M. Phung , K. Pierloot , M. Reiher , I. Schapiro , J. Segarra-Martí , F. Segatta , L. Seijo , S. Sen , D.-C. Sergentu , C. J. Stein , L. Ungur , M. Vacher , A. Valentini and V. Veryazov , Modern quantum chemistry with [Open]Molcas, *J. Chem. Phys.*, 2020, **152** , 214117.

(11) B. O. Roos, P. R. Taylor and P. E. M. Sigbahn, A complete active space SCF method (CASSCF) using a density matrix formulated super-CI approach, *Chem. Phys.*, 1980, **48**, 157-173.

(12) B. O. Roos, V. Veryazov and P.-O. Widmark, Relativistic atomic natural orbital type basis sets for the alkaline and alkaline-earth atoms applied to the ground-state

potentials for the corresponding dimers, *Theor. Chem. Acc.*, 2004, **111**, 345-351.

(13) B. O. Roos, R. Lindh, P.-Å. Malmqvist, V. Veryazov, P.-O. Widmark and A. C. Borin, New Relativistic Atomic Natural Orbital Basis Sets for Lanthanide Atoms with Applications to the Ce Diatom and LuF3, *J. Phys. Chem. A*, 2008, **112**, 11431 -11435.

(14) P. Å. Malmqvist, B. O. Roos and B. Schimmelpfennig, The restricted active space (RAS) state interaction approach with spin–orbit coupling, *Chem. Phys. Lett.*, 2002, **357**, 230-240.

(15) L. F. Chibotaru and L. Ungur, Ab initio calculation of anisotropic magnetic properties of complexes. I. Unique definition of pseudospin Hamiltonians and their derivation, *J. Chem. Phys.*, 2012, **137**, 064112.